

# Structural Similarity-Inspired Unfolding for Lightweight Image Super-Resolution

Zhangkai Ni, *Member, IEEE*, Yang Zhang, Wenhan Yang, *Member, IEEE*,  
Hanli Wang, *Senior Member, IEEE*, Shiqi Wang, *Senior Member, IEEE*, Sam Kwong, *Fellow, IEEE*

**Abstract**—Major efforts in data-driven image super-resolution (SR) primarily focus on expanding the receptive field of the model to better capture contextual information. However, these methods are typically implemented by stacking deeper networks or leveraging transformer-based attention mechanisms, which consequently increases model complexity. In contrast, model-driven methods based on the unfolding paradigm show promise in improving performance while effectively maintaining model compactness through sophisticated module design. Based on these insights, we propose a Structural Similarity-Inspired Unfolding (SSIU) method for efficient image SR. This method is designed through unfolding an SR optimization function constrained by structural similarity, aiming to combine the strengths of both data-driven and model-driven approaches. Our model operates progressively following the unfolding paradigm. Each iteration consists of multiple Mixed-Scale Gating Modules (MSGM) and an Efficient Sparse Attention Module (ESAM). The former implements comprehensive constraints on features, including a structural similarity constraint, while the latter aims to achieve sparse activation. In addition, we design a Mixture-of-Experts-based Feature Selector (MoE-FS) that fully utilizes multi-level feature information by combining features from different steps. Extensive experiments validate the efficacy and efficiency of our unfolding-inspired network. Our model outperforms current state-of-the-art models, boasting lower parameter counts and reduced memory consumption. Our code will be available at: <https://github.com/eezkn/SSIU>

**Index Terms**—Image super-resolution, Light-weight, Paradigm unfolding, Sparse attention

## I. INTRODUCTION

**I**MAGE Super-Resolution (SR) aims to reconstruct High-Resolution (HR) images from Low-Resolution (LR) observations by generating sharp, clear edges and revealing fine texture details while suppressing visual artifacts [1]. It has a wide range of applications, such as improving the image quality to provide a better human visual experience for medical imaging, security inspection, and image compression,

or facilitating downstream computer vision tasks such as object detection and recognition. In recent years, deep learning-based SR methods have gained attention, leveraging large-scale data to obtain the mapping between LR and HR images. One of the most important strategies employed by these methods is the expansion of the network's receptive field. Expanding the receptive field of the network allows it to cover a larger range of input information, significantly improving its capacity to capture long-range dependencies and structural information in the data. Common strategies for enlarging the receptive field include increasing the number of convolutional layers [2], [3], though this can lead to challenges such as vanishing gradients, which calls for the design of additional modules. An alternative approach adopts attention mechanisms [4]–[8], allowing the model to focus on relevant image features and improve SR performance. Transformer-based SR methods [9]–[12] then emerged, effectively leveraging self-attention to capture global information, thus enhancing their ability to perceive contextual cues. These methods expand receptive fields to activate more neighboring pixels, resulting in substantial performance improvements. However, with increasingly complex module designs, these methods often lead to greater network depth and heightened computational and memory demands.

Lightweight SR networks are crucial in mitigating model resource consumption, offering pathways for efficient computation. Various methods have been developed to address specific challenges in this area. Some methods focus on designing lightweight modules [13], [14], while others apply network compression [15] or distillation [16] to derive low-complex models from existing architectures. Another key class of methods enhances training constraints by incorporating domain knowledge, thereby improving the efficiency of module design and integration to reduce the complexity of the model. Notable examples include crafting trainable unfolding networks, as studied in works such as [17]–[19]. These methods combine model-driven domain insights with learning-based paradigms via decomposing complex inverse problems into sequential subtasks, each solved by a dedicated neural network, resulting in end-to-end SR models with enhanced efficiency and performance. From module design optimization to domain knowledge integration, these approaches collectively advance the field, offering efficient and interpretable solutions tailored to lightweight image SR.

From the above reviews, we derive two key insights: 1) Expanding the receptive field is a double-edged sword. While it effectively enhances SR performance, it also significantly increases model complexity. 2) In lightweight SR research,

This work was supported in part by the National Natural Science Foundation of China under Grant 62201387, and Grant 62371343, in part by the Fundamental Research Funds for the Central Universities, and in part by the Interdisciplinary Frontier Research Project of PCL under Grant 2025QYB013. (Corresponding authors: Hanli Wang and Wenhan Yang)

Zhangkai Ni, Yang Zhang, and Hanli Wang are with the School of Computer Science and Technology and the Key Laboratory of Embedded System and Service Computing (Ministry of Education), Tongji University, Shanghai 200092, China (e-mail: zkni@tongji.edu.cn; zhangy\_ce@tongji.edu.cn; hanliwang@tongji.edu.cn).

Shiqi Wang is with the Department of Computer Science, City University of Hong Kong, Hong Kong 999077 (e-mail: shiqwang@cityu.edu.hk).

Wenhan Yang is with Pengcheng Laboratory, Shenzhen, Guangdong 518066, China. (e-mail: yangwh@pcl.ac.cn).

Sam Kwong is with the School of Data Science, Lingnan University, Hong Kong (e-mail: samkwong@ln.edu.hk).

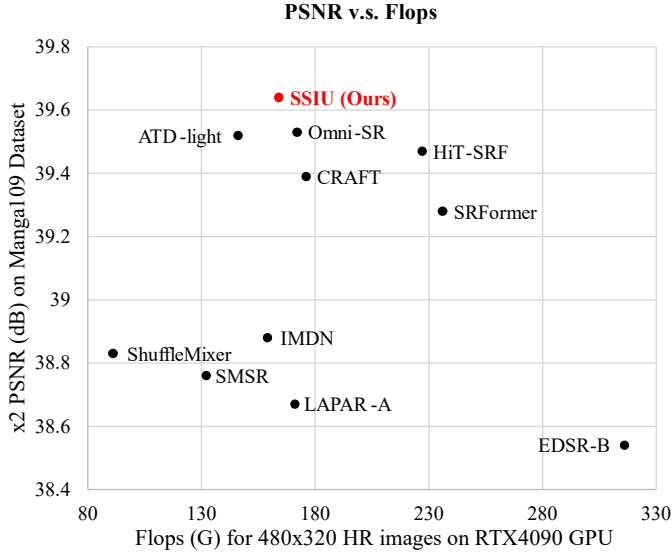


Fig. 1: Performance comparison on the Manga109 dataset. The proposed SSIU model achieves a favorable balanced trade-off between PSNR and FLOPs.

the unfolding paradigm-based approach offers a more general, practical, and interpretable solution. Inspired by these observations, our work introduces the unfolding paradigm to decompose the image SR problem to construct a progressive, trainable, and efficient deep neural network. Specifically, the Maximum A Posteriori (MAP) based image SR problem can be expressed as follows:

$$\mathbf{y} = \mathbf{H}\mathbf{x} + \mathbf{n}, \quad (1)$$

$$\hat{\mathbf{x}} = \arg \min_{\mathbf{x}} \{ \|\mathbf{y} - \mathbf{H}\mathbf{x}\|_2^2 + \lambda p(\mathbf{x}) \}, \quad (2)$$

where  $\mathbf{x}$  is the HR image,  $\mathbf{y}$  is the degraded LR image,  $\mathbf{n}$  represents noise,  $\mathbf{H}$  is a degradation matrix,  $p(\cdot)$  is visual prior regularization term, and  $\hat{\mathbf{x}}$  is the obtained solution. The Equ. (1) formulates the degradation process, and Equ. (2) is the SR estimation process. In Equ. (2), from practical experience,  $\mathbf{H}$  is observed to be local and dynamic, while  $p(\cdot)$  usually presents global context constraint. Several studies have considered solving the inverse problem with these two properties in a unified way. For instance, HAT [20] combines local and global information to activate more distant pixels, leading to improved SR results. Traditional methods based on self-similarity and nonlocal similarity [21] suggest that only structurally similar distant information benefits the SR performance of central pixels. Therefore, we propose a Structural Similarity-Inspired Unfolding network to focus on regions with similar structures to the central pixel with global information aggregation.

Our method achieves a favorable balance between reconstruction performance and computational efficiency by combining the strengths of both convolutional and transformer-based methods, along with data-driven and model-driven approaches, as shown in Fig. 1. Specifically, our network is derived from a typical unfolding-based non-local centralized sparse coding problem. In the progressive solution process, we design a mixed-scale gating module to impose constraints

on feature representation and a sparse attention mechanism to achieve efficient sparse activation. Additionally, we introduce a mixture-of-experts-based feature selector for gating features from different scales. This progressive framework and the three proposed modules efficiently integrate global and local information, improving SR performance while maintaining a lightweight architecture. In summary, the key contributions are as follows:

- We propose a novel Structural Similarity-Inspired Unfolding (SSIU) network for lightweight image SR, which sparsely activates long-range pixels, leading to improved SR results with a lightweight architecture.
- We design a Mixed-Scale Gating Module (MSGM) to impose sparsity and structural similarity constraints, and an Efficient Sparse Attention Module (ESAM) to reduce the complexity of long-range modeling.
- We introduce a Mixture-of-Experts Feature Selector (MoE-FS) that effectively integrates multi-scale features using a learnable gating mechanism. Extensive experiments show that SSIU outperforms state-of-the-art models, achieving better SR performance with faster inference and lower memory usage.

The rest of this paper is organized as follows. Section II provides a concise review of related work. Section III details the proposed SSIU model. Section IV presents the experimental results. Section V concludes the paper.

## II. RELATED WORKS

### A. Deep Networks for Image Super-Resolution

With the advent of deep learning, CNN-based SR models [1]–[3], [7], [8], [22], [23] have become the prevailing approach. Dong et al. introduced SRCNN [1], the first CNN-based SR network, which outperformed traditional methods and laid the groundwork for deep SR. VDSR [2] then employed a very deep network to achieve high-precision reconstruction. DeFiAN [7] incorporated a fidelity attention mechanism to adaptively enhance both high-frequency details and low-frequency smoothness. TDPN [3] added a texture-guided branch to improve perceptual quality, and FDSR [8] operates in the frequency domain by dividing images into distinct frequency bands for targeted reconstruction. Although CNN-based methods have advantages in terms of computational complexity, their performance is insufficient.

Based on Vision Transformer (ViT) [24], several methods [10], [11], [20], [25]–[27] have explored Transformer-based SR. TTSR [25] proposed the first Transformer-based SR model, using hard and soft attention modules for reference-based SR. SwinIR [11] advanced SR by combining the Swin Transformer’s local window self-attention with convolutional operations. ESRT [10] optimized the structure of the Transformer by fusing CNN and Transformer features to reduce complexity and improve performance. HAT [20] improved performance by integrating channel attention with self-attention, introducing an overlapping cross-attention module and a pre-training strategy. ACT [26] proposed a parallel CNN-Transformer architecture based on cross-scale attention for extracting both local and global features. ATD [27] introduced

an adaptive token dictionary to recover lost high-quality details. Despite these advancements, Transformer-based models still demand considerable resources due to the computational cost of the self-attention mechanism. Inspired by recent image enhancement studies [28], [29], several works have explored the integration of diffusion models into SR [30], [31]. ACDMSR [30] introduced a diffusion-based SR framework that leverages a pre-trained SR model to provide improved conditional inputs. SinSR [31] accelerated the diffusion-based SR model to a single inference step based on a deterministic sampling process.

### B. Lightweight Networks for Image Super-Resolution

To reduce model resource consumption, various CNN-based methods have been developed [32]–[38]. These include EDSR [32], which simplifies residual networks by removing unnecessary modules; CARN [33], which adopts a cascaded residual structure; and IMDN [34], which utilizes multi-distillation for faster inference. LAPAR [35] formulates SR as a linear regression problem for efficient enhancement, while ECBSR [36] focuses on edge-aware lightweight design for mobile devices. SMSR [37] leverages sparse masking for computational efficiency, and ShuffleMixer [38] explores large-kernel convolutions and channel splitting. However, CNN-based methods are inherently limited by local receptive fields, which constrain their capacity for long-range modeling.

Motivated by the strong capability of Transformers in capturing global dependencies, a series of recent works [39]–[44] have investigated their use in enhancing image SR performance. LBNNet [39] combines a symmetric CNN and a recursive Transformer to extract local features and long-range dependencies, effectively balancing performance and computational cost. SRFormer [40] proposes a permuted self-attention mechanism that shifts spatial information into the channel dimension, reducing the overhead introduced by large attention windows. CRAFT [41] incorporates high-frequency priors to guide SR, thereby simplifying network design. SAFMN [42] replaces multi-head attention with a multi-scale feature modulation module to reduce computational burden. Omni-SR [43] adopts a full self-attention scheme to model spatial and channel interactions jointly, achieving both lightweight design and improved performance. HiT-SR [44] introduces a hierarchical Transformer to capture multi-scale features and long-range dependencies, further boosting SR quality. Although these methods reduce complexity through architectural innovations, they primarily concentrate on network design rather than explicitly modeling the SR reconstruction process to achieve further efficiency improvements.

## III. STRUCTURAL SIMILARITY-INSPIRED UNFOLDING NETWORK

### A. Problem Formulation

We formulate the image SR problem as a MAP estimation problem with structural similarity constraints. Given an LR image  $\mathbf{y}$  and an HR image  $\mathbf{x}$ , the image SR process can be expressed using MAP estimation, as shown in Equ. (2). Following the setting of the Sparse Coding (SC) model [21],

we simplify the MAP estimation problem into a sparse coding problem based on the  $L_1$ -norm:

$$\alpha_{\mathbf{x}} = \arg \min_{\alpha} \{ \|\mathbf{y} - \mathbf{H}\Phi\alpha\|_2^2 + \lambda \|\alpha\|_1 \}, \quad (3)$$

where  $\Phi$  is a signal dictionary with signal atoms that help reconstruct the HR images.  $\alpha$  is the sparse coding coefficient representing the weight of dictionary atoms,  $\alpha_{\mathbf{x}}$  is the predicted sparse coding coefficient, and  $\lambda$  is the weighting parameter. The predicted HR image  $\hat{\mathbf{x}}$  can be obtained using  $\alpha_{\mathbf{x}}$  and  $\Phi$ :  $\hat{\mathbf{x}} = \Phi\alpha_{\mathbf{x}}$ . Inspired by the traditional methods of using non-local similarity [45], we further impose structural similarity constraints on the coefficient  $\alpha$  to pay more attention to the information of structurally similar regions:

$$\alpha_{\mathbf{x}} = \arg \min_{\alpha} \{ \|\mathbf{y} - \mathbf{H}\Phi\alpha\|_2^2 + \lambda \|\alpha\|_1 + \gamma \|\alpha - \beta\|_1 \}, \quad (4)$$

where the coefficient  $\beta$  is a variable estimated from  $\alpha$  based on structural similarity, and  $\gamma$  is a weighting parameter. To facilitate optimization, we introduce an auxiliary variable  $\mathbf{z}$  to replace  $\alpha$ , resulting in the following optimization problem:

$$\alpha_{\mathbf{x}} = \arg \min_{\alpha} \{ \|\mathbf{y} - \mathbf{H}\Phi\alpha\|_2^2 + \lambda \|\mathbf{z}\|_1 + \gamma \|\alpha - \beta\|_1 + \eta \|\mathbf{z} - \alpha\|_2 \}, \quad (5)$$

where  $\eta$  is a weighting parameter.

To solve the optimization problem in Equ. (5), we employ an alternating optimization approach where the value of one variable is updated while keeping the other variables fixed. This approach partitions the problem into three univariate subproblems, which can be optimized using the following alternating scheme at stage  $t+1$ :

$$\begin{aligned} (P1) \quad \mathbf{z}^{t+1} &= \arg \min_{\mathbf{z}} \{ \lambda \|\mathbf{z}\|_1 + \eta \|\mathbf{z} - \alpha^t\|_2 \}, \\ (P2) \quad \beta^{t+1} &= \arg \min_{\beta} \{ \gamma \|\alpha^t - \beta\|_1 \}, \\ (P3) \quad \alpha^{t+1} &= \arg \min_{\alpha} \{ \|\mathbf{y} - \mathbf{H}\Phi\alpha\|_2^2 + \gamma \|\alpha - \beta^{t+1}\|_1 \\ &\quad + \eta \|\mathbf{z}^{t+1} - \alpha\|_2 \}. \end{aligned}$$

Thus, an iterative solution can be obtained to update  $\mathbf{z}^t$ ,  $\beta^t$  and  $\alpha^t$  sequentially with Half Quadratic Splitting (HQS) [46]:

$$\begin{aligned} (S1) \quad \mathbf{z}^{t+1} &= S_{\tau_1}(\alpha^t), \\ (S2) \quad \beta^{t+1} &= S_{\tau_2}(\alpha^t), \\ (S3.a) \quad \mathbf{v}^{t+1} &= \omega_1 \mathbf{z}^{t+1} + \omega_2 \mathbf{K}^T (\mathbf{y} - \mathbf{K} \cdot \alpha^t) / c + \alpha^t, \\ (S3.b) \quad \alpha^{t+1} &= S_{\tau_3}(\mathbf{v}^{t+1} - \beta^{t+1}) + \beta^{t+1}, \end{aligned}$$

where  $S_{\tau}(\cdot)$  is the soft threshold operator, representing the solution process.  $\tau_1$ ,  $\tau_2$ , and  $\tau_3$  are hyperparameters related to the constraints.  $\mathbf{v}$  is an intermediate variable to facilitate the description of subproblem (S3).  $\mathbf{K} = \mathbf{H}\Phi$ ,  $\mathbf{K}^T = \Phi^T \mathbf{H}^T$ ,  $\mathbf{T}$  represents the transpose operation.  $\omega_1$  and  $\omega_2$  are weighting parameters and  $c$  is an auxiliary parameter guaranteeing the convexity of the surrogate function [47]. In summary, (S1) applies a sparse constraint on  $\alpha$  and (S2) imposes structural similarity constraint. Then (S3.a) performs a global sparse inverse-solving process and (S3.b) centralizes the estimation to  $\alpha^{t+1}$ . Finally, after  $N$  iterations, we have  $\alpha_{\mathbf{x}} = \alpha^N$ , and the corresponding SR result is  $\hat{\mathbf{x}} = \Phi\alpha_{\mathbf{x}}$ .

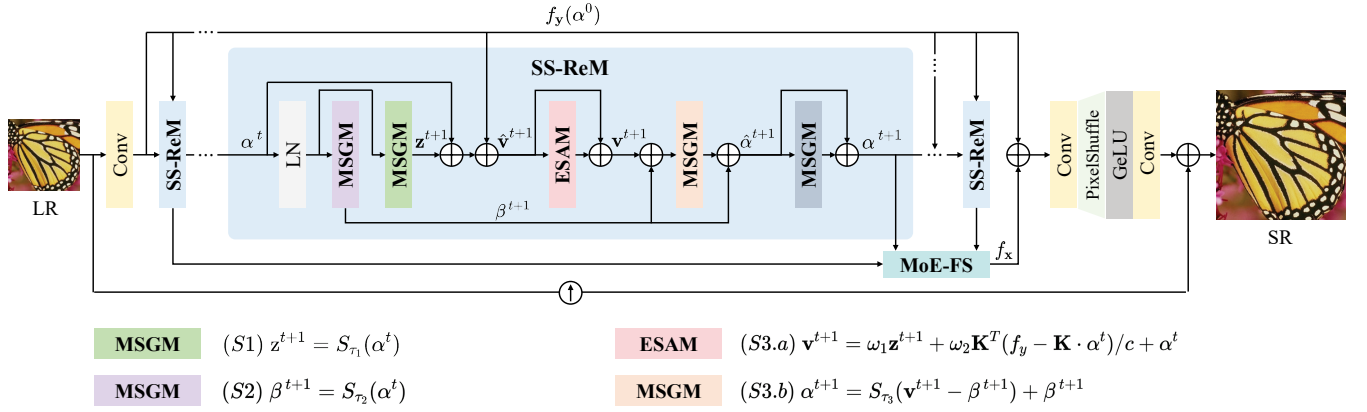


Fig. 2: Overall pipeline of the SSIU. It progressively refines features using the Structural Similarity-Inspired Recurrent Module (SS-ReM), which integrates Mixed-Scale Gating Modules (MSGM) for sparsity and structural similarity constraints, and the Efficient Sparse Attention Module (ESAM) for efficient long-range modeling. The Mixture-of-Experts-based Feature Selector (MoE-FS) further refines feature by gating outputs from multiple SS-ReM modules. For simplicity, we retain the symbols  $\alpha$ ,  $\beta$ ,  $v$ , and  $z$  to represent their corresponding features, while converting only the input  $y$  into the feature representation  $f_y$ .

Inspired by the above solution, we follow the general route of the processes (S1, S2, S3) to construct our network. It is worth noting that the solution of the above unfolding paradigm is performed in the image space, and the LR image  $y$  participates in the solution process. In this paper, we use the unfolding paradigm in the feature space. The feature space retains the key structural information of the image space, ensuring that the above solution still holds. To simplify the symbolic representation, we continue to use  $\alpha$ ,  $\beta$ ,  $v$ ,  $z$  to represent the corresponding features and only convert the input  $y$  into the feature  $f_y$ . As illustrated in Fig. 2, our proposed model performs the following process at each stage  $t + 1$ :

- **S1:** We impose a sparse constraint on the feature  $\alpha^t$  from the previous stage to update  $z^t$ . This operation is simulated using a mixed-scale gating module (MSGM).
- **S2:** The feature  $\alpha^t$  is fed into another MSGM to obtain the estimate  $\beta^{t+1}$  of  $\alpha^t$  based on structural similarity.
- **S3.a:** The feature  $\alpha^t$ , the feature  $z^{t+1}$  from S1, and the feature  $f_y$  extracted from  $y$  are processed and fused through an efficient sparse self-attention module (ESAM).
- **S3.b:** Aggregate the constraints on feature  $v^{t+1}$  and feature  $\beta^{t+1}$  onto feature  $\alpha^{t+1}$  through MSGM.

It is noted that we use the same module MSGM to solve subproblems S1, S2, and S3.b as the essence of these three subproblems lies in performing a linear transformation on the input followed by thresholding. Our MSGM is implemented based on a gating mechanism, which can achieve all targets of sparsity constraints, structural similarity constraints, and feature aggregation by dynamically adjusting the weights of input features.

### B. Overview of SSIU

The overall pipeline of SSIU is illustrated in Fig. 2, consisting of three key components: **Shallow Feature Extraction**, **Progressive Feature Refinement**, and **HR Image Reconstruction**, which are detailed as follows:

1) *Shallow Feature Extraction:* Given an LR image  $y \in R^{3 \times h \times w}$  with spatial resolution  $h \times w$ , it is first embedded into feature  $f_y \in R^{C \times H \times W}$  through a shallow feature extraction module  $M_{FE}(\cdot)$ .  $C$  denotes the number of feature channels and  $H \times W$  is the feature spatial resolution:

$$f_y = M_{FE}(y), \quad (6)$$

where  $M_{FE}(\cdot)$  consists of a  $3 \times 3$  convolution.

2) *Progressive Feature Refinement:* We perform progressive feature refinement using stacked Structural Similarity-Inspired Recurrent Modules (SS-ReM) to transform LR features into HR features. Each SS-ReM takes  $\alpha$  and  $f_y$  as input and outputs the updated  $\alpha$ :

$$\alpha^{t+1} = \text{SS-ReM}_t(\alpha^t, f_y), \quad t = 0, 1, \dots, N - 1, \quad (7)$$

where  $\alpha^t$  is the output of the previous SS-ReM module, and  $\alpha^0$  is initialized with the shallow features  $f_y$ .  $N$  means the number of SS-ReM and is set to 9 in this paper.  $\beta^t$ ,  $v^t$  and  $z^t$  are optimized by SS-ReM during the update process of  $\alpha^t$ . In addition, rather than directly using the final output  $\alpha^N$  from the last module, our method combines multi-level features, as their distinct characteristics lead to better enhancement results. Therefore, we introduce a Mixture-of-Experts-based Feature Selector (MoE-FS), which learns to gate the features  $\alpha^t$  from multiple stages to produce the final feature  $f_x \in R^{C \times H \times W}$ :

$$f_x = \text{MoE-FS}(\alpha^1, \dots, \alpha^N). \quad (8)$$

In order to balance the model performance and computational complexity, we only select 3 outputs of SS-ReM as the inputs of MoE-FS during implementation.

3) *HR Image Reconstruction:* The progressively refined features  $f_x$  are combined with the  $f_y$  to reconstruct the SR image. Instead of learning the direct mapping from the LR image to the HR image, our model employs a reconstruction module  $M_{RC}(\cdot)$  to generate the residual image. The  $M_{RC}(\cdot)$  contains a  $1 \times 1$  convolutional layer, a pixel shuffle layer, a

GeLU activation layer, and a  $3 \times 3$  convolutional layer. This process can be expressed as follows:

$$\hat{\mathbf{x}} = \text{M}_{\text{RC}}(f_{\mathbf{x}} + f_{\mathbf{y}}) + \Gamma(\mathbf{y}), \quad (9)$$

where  $\Gamma(\cdot)$  denotes bilinear upsampling,  $\hat{\mathbf{x}} \in R^{3 \times hs \times ws}$  is the final reconstructed image, and  $s$  represents the SR scale. The proposed SSIU achieves an excellent trade-off between computational overhead and reconstruction quality.

### C. Structural Similarity-Inspired Recurrent Module

The stacked SS-ReMs are used to implement the progressive feature refinement process. As shown in Fig. 2, each SS-ReM consists of several MSGM and an ESAM, corresponding to the steps ( $S1, S2, S3$ ). Specifically, the feature  $\alpha^t$  is processed by an MSGM after layer normalization (LN), imposing a sparsity constraint and yielding an updated auxiliary variable  $\mathbf{z}^{t+1}$ :

$$\mathbf{z}^{t+1} = S_{\tau_1}(\alpha^t) = \text{MSGM}_1(\text{LN}(\alpha^t)). \quad (10)$$

Simultaneously,  $\alpha^t$  is also input into another MSGM to obtain an estimate  $\beta^{t+1}$  with structural similarity constraint:

$$\beta^{t+1} = S_{\tau_2}(\alpha^t) = \text{MSGM}_2(\text{LN}(\alpha^t)). \quad (11)$$

Next, an ESAM is used to perform sparse activation on  $\mathbf{z}^{t+1}$ ,  $\alpha^t$ , and  $f_{\mathbf{y}}$  to obtain the updated intermediate variable  $\mathbf{v}^{t+1}$ . To simplify this module, we first sum the inputs into  $\hat{\mathbf{v}}^{t+1}$  and then feed it into ESAM with a skip connection:

$$\begin{aligned} \hat{\mathbf{v}}^{t+1} &= \mathbf{z}^{t+1} + \alpha^t + f_{\mathbf{y}}, \\ \mathbf{v}^{t+1} &= \text{ESAM}(\hat{\mathbf{v}}^{t+1}) + \hat{\mathbf{v}}^{t+1}. \end{aligned} \quad (12)$$

$\mathbf{v}^{t+1}$  is a combination of three features  $\mathbf{z}^{t+1}$ ,  $\alpha^t$ , and  $f_{\mathbf{y}}$ , which is essentially the same as  $S3.a$ . Subsequently,  $\mathbf{v}^{t+1}$  and  $\beta^{t+1}$  are input into an MSGM for feature aggregation to obtain feature  $\hat{\alpha}^{t+1}$  with structural similarity constraint and sparse activation. Following  $S3.b$ , we input the sum of  $\mathbf{v}^{t+1}$  and  $\beta^{t+1}$  into MSGM and add the output to  $\beta^{t+1}$ :

$$\begin{aligned} \hat{\alpha}^{t+1} &= S_{\tau_3}(\mathbf{v}^{t+1} + \beta^{t+1}) + \beta^{t+1} \\ &= \text{MSGM}_3(\mathbf{v}^{t+1} + \beta^{t+1}) + \beta^{t+1}. \end{aligned} \quad (13)$$

Finally, to further improve the model performance,  $\hat{\alpha}^{t+1}$  is input into an MSGM-based Feedforward Network (FFN) for feature refinement:

$$\alpha^{t+1} = \text{MSGM}_4(\hat{\alpha}^{t+1}) + \hat{\alpha}^{t+1}. \quad (14)$$

### D. Mixed-Scale Gating Module

As shown in Fig. 3, the proposed MSGM enhances features by integrating multi-scale representation and a gating mechanism [48]. Given a feature  $f_m \in R^{C \times H \times W}$ , it is processed through parallel branches to capture information at different scales. One branch applies a  $1 \times 1$  convolution, while the other incorporates depth-wise convolution (DWConv) between two  $1 \times 1$  convolutions. The output feature  $\hat{f}_1$  of the first branch is processed through a GeLU activation function. Then the activated  $\hat{f}_1$  is element-wise multiplied with the output feature  $\hat{f}_2$  of the second branch to gate  $\hat{f}_2$ , allowing it to retain relevant

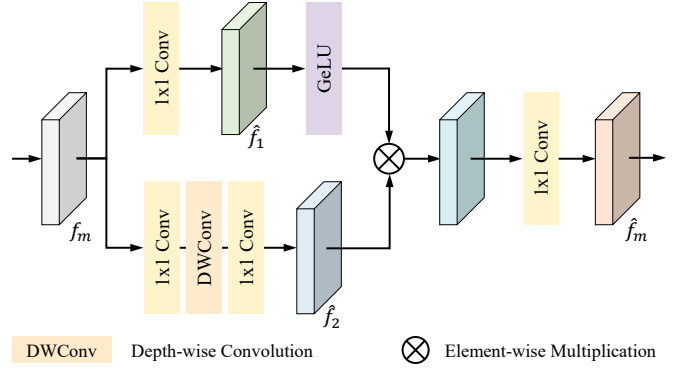


Fig. 3: Details of the proposed MSGM.

information while suppressing irrelevant parts. The result is then refined through a  $1 \times 1$  convolution:

$$\begin{aligned} \hat{f}_1 &= \text{Conv}(f_m), \\ \hat{f}_2 &= \text{Conv}(\text{DWConv}(\text{Conv}(f_m))), \\ \hat{f}_m &= \text{Conv}(\sigma(\hat{f}_1) \cdot \hat{f}_2), \end{aligned} \quad (15)$$

where  $\sigma$  denotes a GeLU activation function,  $\text{Conv}(\cdot)$  denotes a  $1 \times 1$  convolution and  $\cdot$  means element-wise multiplication.

### E. Efficient Sparse Attention Module

Traditional transformers use all features for self-attention calculations, leading to high computational complexity and memory consumption [49]. However, previous works [45], [50] show that only the interconnection between structurally similar patches is beneficial. This insight provides a promising opportunity to expand the receptive field while reducing computational complexity, which we efficiently achieve by introducing ESAM. The input feature  $f_e \in R^{C \times H \times W}$  is first down-sampled using sparse sampling, yielding  $X \in R^{C \times H_1 \times W_1}$ :

$$X = \text{Sparse}(f_e), \quad (16)$$

where  $\text{Sparse}(\cdot)$  operation is implemented using max-pooling, and  $H_1 \times W_1$  is the spatial dimension of  $X$ . The downsampled feature  $X$  is then reshaped into  $X' \in R^{C \times ((\frac{H_1-M}{M-O}+1) \times (\frac{W_1-M}{M-O}+1)) \times M^2}$  by partitioning  $X$  into overlapping  $M \times M$  blocks with overlap size  $O$ . Here,  $(\frac{H_1-M}{M-O}+1) \times (\frac{W_1-M}{M-O}+1)$  denotes the total number of blocks. Following this, standard self-attention is computed using  $X'$ :

$$Y = \text{Softmax}\left(\frac{Q \cdot K^T}{\sqrt{d_k}}\right) \cdot V, \quad (17)$$

where  $Q = P_Q(X')$ ,  $K = P_K(X')$ , and  $V = P_V(X')$ .  $P_Q(\cdot)$ ,  $P_K(\cdot)$  and  $P_V(\cdot)$  are convolutional layers with the kernel size  $1 \times 1$  and  $d_k$  is the dimension of  $K$ . Finally, the result  $Y$  is enhanced by a  $3 \times 3$  convolution layer and then upsampled back to its original size:

$$\hat{f}_e = \Gamma(\Psi(Y)), \quad (18)$$

where  $\Psi(\cdot)$  is a  $3 \times 3$  convolution layer and  $\Gamma(\cdot)$  denotes bilinear upsampling.



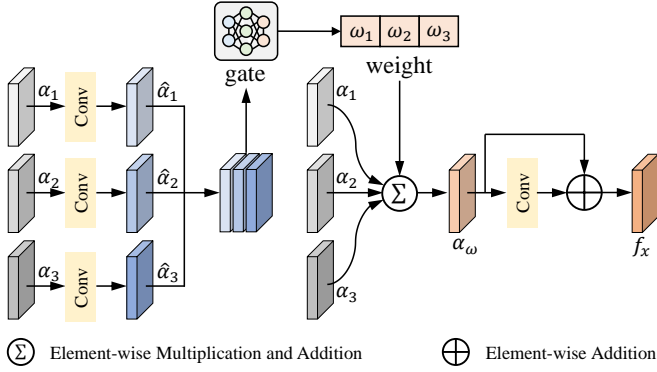


Fig. 4: Details of the proposed MoE-FS.

### F. Mixture-of-Experts based Feature Selector

The proposed MoE-FS uses a learning-based gating module to integrate features from multiple levels as experts, as illustrated in Fig. 4. Using the output  $\alpha^t$  from the SS-ReM modules as input, MoE-FS combines the distinct characteristics of features from different levels. As mentioned above, we only select 3 features for input. Specifically, we divide the stacked SS-ReM into three groups, corresponding to the encoding block, bottleneck block, and decoding block, and take the output of each block as the final inputs, denoted as  $\alpha_1$ ,  $\alpha_2$ , and  $\alpha_3$ . The features are first processed by a  $1 \times 1$  convolution and fed to the gating module to calculate the feature weights:

$$\begin{aligned} \hat{\alpha}_i &= \text{Conv}_i(\alpha_i), \quad i = 1, 2, 3, \\ \{\omega_1, \omega_2, \omega_3\} &= \text{Softmax}(\{\hat{\alpha}_1, \hat{\alpha}_2, \hat{\alpha}_3\}), \end{aligned} \quad (19)$$

where  $\{\cdot\}$  denotes the concatenation operation. These features are gated based on their corresponding weights to compute the weighted sum  $\alpha_\omega$ . It is then passed through a residual block with a  $1 \times 1$  convolution for feature fusion, resulting in the final output feature  $f_x$ :

$$\begin{aligned} \alpha_\omega &= \alpha_1\omega_1 + \alpha_2\omega_2 + \alpha_3\omega_3, \\ f_x &= \alpha_\omega + \text{Conv}(\alpha_\omega). \end{aligned} \quad (20)$$

### G. Training Objectives

The proposed SSIU is optimized using the objective:

$$L = L_1 + \lambda L_f, \quad (21)$$

where  $L_1$  measures the  $L_1$  distance between the SR result and the ground truth, and  $L_f$  computes the  $L_1$  distance between their Fast Fourier Transforms (FFT)-transformed versions. The constant  $\lambda$  balances the relative importance of  $L_f$ .

## IV. EXPERIMENT

### A. Experimental Setup

1) *Dataset*: Following previous works [35], [38], we train our model on the DF2K dataset, which combines DIV2K [51] and Flickr2K [32], resulting in a total of 3,450 high-quality images (800 from DIV2K and 2,650 from Flickr2K). The LR images are generated by applying bicubic downscaling

to the corresponding HR images. To thoroughly assess our method's performance, we perform evaluations on five widely-used benchmark datasets: Set5 [52], Set14 [53], BSD100 [54], Urban100 [55], and Manga109 [56].

2) *Implementation Details*: In the proposed SSIU, we employ SS-ReM modules with 64 feature channels. For training, 40 patches of size  $64 \times 64$  are randomly cropped from LR images and paired with corresponding HR patches. These training patch pairs are augmented by random horizontal flipping and rotation. The proposed model is trained using the Adam optimizer [57]. The learning rate is initialized at  $1e-3$  and decays to  $1e-6$  following the Cosine Annealing schedule [58]. The  $\lambda$  is set to 0.01 in all of our experiments. All experiments are conducted with the PyTorch framework on an NVIDIA GeForce RTX 4090 GPU.

3) *Benchmarks*: To comprehensively evaluate the performance of the proposed SSIU, we compare it with classic and state-of-the-art lightweight SR models, including CARN [33], EDSR-baseline [32], IMDN [34], ECBSR [36], SMSR [37], LBNNet [39], SRFormer [40], CRAFT [41], HiT-SRF [44], ATD-light [27], LAPAR [35], ShuffleMixer [38], SAFMN [42], and Omni-SR [43].

4) *Evaluation Metrics*: To assess the quality of the SR images, we employ peak signal-to-noise ratio (PSNR) and structural similarity index (SSIM) metrics. Following the setting of existing works, all PSNR and SSIM values are computed based on the luminance (Y) channel of the images in the YCbCr color space. PSNR evaluates the quality in terms of fidelity, while SSIM focuses on perceptual quality.

### B. Comparisons with State-of-the-Art Methods

1) *Quantitative Comparison*: Table I presents quantitative comparisons of various SR models for upscaling factors  $\times 2$ ,  $\times 3$ , and  $\times 4$  on five widely used benchmark datasets. It provides details on the number of model parameters, floating-point operations (FLOPs), and training datasets for each model. The FLOPs are calculated based on the SR of an image of  $1280 \times 720$  pixels. The proposed SSIU model, leveraging structural similarity-inspired SR optimization and the efficient SS-ReM, demonstrates superior performance with reduced parameters and lower computational complexity. Several critical conclusions can be drawn from Table I. Firstly, compared to classic and state-of-the-art lightweight SR algorithms, SSIU achieves better performance with similar parameters and FLOPs. Particularly, for  $\times 4$  SR on the Manga109 dataset, the performance gain of the proposed SSIU over LBNNet, CRAFT, and ATD-light is 0.76dB, 0.25dB, and 0.12dB, respectively. Secondly, for the  $\times 2$  upscaling factor, SSIU performs competitively against SRFormer, Omni-SR, and HiT-SRF, while requiring fewer parameters or FLOPs. Although models like ShuffleMixer and SAFMN have fewer parameters, SSIU significantly outperforms them on all benchmark datasets. Finally, for  $\times 3$  and  $\times 4$  upscaling, SSIU consistently achieves superior or competitive performance across all datasets. Overall, the results in Table I demonstrate that SSIU offers a compelling trade-off between efficiency and reconstruction quality compared to existing state-of-the-art methods.

TABLE I: Performance comparison of various lightweight SR models on five widely used benchmark datasets. All PSNR/SSIM values are computed on the Y-channel of the YCbCr color space. The FLOPs are measured corresponding to an SR image of size  $1280 \times 720$  pixels. The top three performances are highlighted in red, orange, and yellow backgrounds, respectively.

Method	Training Dataset	Scale	Param. [K]	FLOPs [G]	Set5 PSNR/SSIM	Set14 PSNR/SSIM	BSD100 PSNR/SSIM	Urban100 PSNR/SSIM	Manga109 PSNR/SSIM
CARN [33]	DIV2K	$\times 2$	1,592	223	37.76/0.9590	33.52/0.9166	32.09/0.8978	31.92/0.9256	38.36/0.9765
EDSR-B [32]	DIV2K		1,370	316	37.99/0.9604	33.57/0.9175	32.16/0.8994	31.98/0.9272	38.54/0.9769
IMDN [34]	DIV2K		694	159	38.00/0.9605	33.63/0.9177	32.19/0.8996	32.17/0.9283	38.88/0.9774
ECBSR-M [36]	DIV2K		596	137	37.90/0.9615	33.34/0.9178	32.10/0.9018	31.71/0.9250	-
SMSR [37]	DIV2K		985	132	38.00/0.9601	33.64/0.9179	32.17/0.8990	32.19/0.9284	38.76/0.9771
LBNNet [39]	DIV2K		731	153	38.05/0.9607	33.65/0.9177	32.16/0.8994	32.30/0.9291	38.88/0.9775
SRFormer [40]	DIV2K		853	236	38.23/0.9613	33.94/0.9209	32.36/0.9019	32.91/0.9353	39.28/0.9785
CRAFT [41]	DIV2K		737	176	38.23/0.9615	33.92/0.9211	32.33/0.9016	32.86/0.9343	39.39/0.9786
HiT-SRF [44]	DIV2K		847	227	38.26/0.9615	34.01/0.9214	32.37/0.9023	33.13/0.9372	39.47/0.9787
ATD-light [27]	DIV2K		753	146	38.29/0.9616	34.10/0.9217	32.39/0.9023	33.27/0.9375	39.52/0.9789
LAPAR-A [35]	DF2K		548	171	38.01/0.9605	33.62/0.9183	32.19/0.8999	32.10/0.9283	38.67/0.9772
ShuffleMixer [38]	DF2K		394	91	38.01/0.9606	33.63/0.9180	32.17/0.8995	31.89/0.9257	38.83/0.9774
SAFMN [42]	DF2K		228	52	38.00/0.9605	33.54/0.9177	32.16/0.8995	31.84/0.9256	38.71/0.9771
Omni-SR [43]	DF2K		772	172	38.29/0.9617	34.27/0.9238	32.41/0.9026	33.30/0.9386	39.53/0.9792
Ours	DF2K		778	164	38.31/0.9632	34.20/0.9255	32.43/0.9043	33.25/0.9393	39.64/0.9822
CARN [33]	DIV2K	$\times 3$	1,592	119	34.29/0.9255	30.29/0.8407	29.06/0.8034	28.06/0.8493	33.50/0.9440
EDSR-B [32]	DIV2K		1,555	160	34.37/0.9270	30.28/0.8417	29.09/0.8052	28.15/0.8527	33.45/0.9439
IMDN [34]	DIV2K		703	72	34.36/0.9270	30.32/0.8417	29.09/0.8046	28.17/0.8519	33.61/0.9445
SMSR [37]	DIV2K		993	68	34.40/0.9270	30.33/0.8412	29.10/0.8050	28.25/0.8536	33.68/0.9445
LBNNet [39]	DIV2K		736	68	34.47/0.9277	30.38/0.8417	29.13/0.8061	28.42/0.8559	33.82/0.9460
SRFormer [40]	DIV2K		861	105	34.67/0.9296	30.57/0.8469	29.26/0.8099	28.81/0.8655	34.19/0.9489
CRAFT [41]	DIV2K		744	78	34.71/0.9295	30.61/0.8469	29.24/0.8093	28.77/0.8635	34.29/0.9491
HiT-SRF [44]	DIV2K		855	102	34.75/0.9300	30.61/0.8475	29.29/0.8106	28.99/0.8687	34.53/0.9502
ATD-light [27]	DIV2K		760	65	34.74/0.9300	30.68/0.8485	29.32/0.8109	29.17/0.8709	34.60/0.9506
LAPAR-A [35]	DF2K		594	114	34.36/0.9267	30.34/0.8421	29.11/0.8054	28.15/0.8523	33.51/0.9441
ShuffleMixer [38]	DF2K		415	43	34.40/0.9272	30.37/0.8423	29.12/0.8051	28.08/0.8498	33.69/0.9448
SAFMN [42]	DF2K		233	23	34.34/0.9267	30.33/0.8418	29.08/0.8048	27.95/0.8474	33.52/0.9437
Omni-SR [43]	DF2K		780	78	34.77/0.9304	30.70/0.8489	29.33/0.8111	29.12/0.8712	34.64/0.9507
Ours	DF2K		799	75	34.79/0.9323	30.71/0.8523	29.35/0.8138	29.08/0.8718	34.73/0.9547
CARN [33]	DIV2K	$\times 4$	1,592	91	32.13/0.8937	28.60/0.7806	27.58/0.7349	26.07/0.7837	30.47/0.9084
EDSR-B [32]	DIV2K		1,518	114	32.09/0.8938	28.58/0.7813	27.57/0.7357	26.04/0.7849	30.35/0.9067
IMDN [34]	DIV2K		715	41	32.21/0.8948	28.58/0.7811	27.56/0.7353	26.04/0.7838	30.45/0.9075
ECBSR-M [36]	DIV2K		603	35	31.92/0.8946	28.34/0.7817	27.48/0.7393	25.81/0.7773	-
SMSR [37]	DIV2K		1006	42	32.12/0.8932	28.55/0.7808	27.55/0.7351	26.11/0.7868	30.54/0.9085
LBNNet [39]	DIV2K		742	39	32.29/0.8960	28.68/0.7832	27.62/0.7382	26.27/0.7906	30.76/0.9111
SRFormer [40]	DIV2K		873	63	32.51/0.8988	28.82/0.7872	27.73/0.7422	26.67/0.8032	31.17/0.9165
CRAFT [41]	DIV2K		753	47	32.52/0.8989	28.85/0.7872	27.72/0.7418	26.56/0.7995	31.18/0.9168
HiT-SRF [44]	DIV2K		866	58	32.55/0.8999	28.87/0.7880	27.75/0.7432	26.80/0.8069	31.26/0.9171
ATD-light [27]	DIV2K		769	39	32.63/0.8998	28.89/0.7886	27.79/0.7440	26.97/0.8107	31.48/0.9198
LAPAR-A [35]	DF2K		659	94	32.15/0.8944	28.61/0.7818	27.61/0.7366	26.14/0.7871	30.42/0.9074
ShuffleMixer [38]	DF2K		411	28	32.21/0.8953	28.66/0.7827	27.61/0.7366	26.08/0.7835	30.65/0.9093
SAFMN [42]	DF2K		240	14	32.18/0.8948	28.60/0.7813	27.58/0.7359	25.97/0.7809	30.43/0.9063
Omni-SR [43]	DF2K		792	45	32.57/0.8993	28.95/0.7898	27.81/0.7439	26.95/0.8105	31.50/0.9192
Ours	DF2K		794	49	32.64/0.9032	28.96/0.7939	27.82/0.7472	26.83/0.8098	31.60/0.9242

2) *Qualitative Comparison*: The visual comparison results of the  $\times 4$  upscaling factor on the Set14, Urban100, B100, and Manga109 datasets are presented in Fig. 5, Fig. 6, Fig. 7, and Fig. 8, with the zoomed-in detail results. The qualitative comparison highlights that our proposed SSIU consistently produces sharper edges, enhanced structures, and textures. Specifically, from Fig. 5 to Fig. 8, we observe that SSIU generates more accurate details compared to other methods, particularly in lines and structures. This highlights SSIU's superior performance in preserving and enhancing crucial features in upscaled images, further validating the effectiveness of the structural similarity-inspired unfolding framework, which enables our model to capture and refine complex structural details in SR images.

3) *Inference Time*: To demonstrate the computational efficiency of our method, we compare the peak GPU memory

TABLE II: PSNR (dB), Memory Usage (M), and Inference Time (ms) Comparison for  $\times 4$  SR. GPU Mem. is the peak GPU memory consumption during inference, while Avg. Time is the average processing time for 100 SR images of size  $480 \times 320$  pixels.

Metrics	SRFormer	CRAFT	Omni-SR	HiT-SRT	ATD-light	SSIU(Ours)
PSNR	27.73	27.72	27.81	27.75	27.79	27.82
GPU Mem.	4181	1586	1597	1878	753	224
Avg. Time	42.58	33.94	19.61	47.96	41.97	13.83

consumption and the average inference time with several state-of-the-art approaches that have comparable parameter sizes. Specifically, the maximum GPU memory usage refers to the highest memory consumed during inference, and the

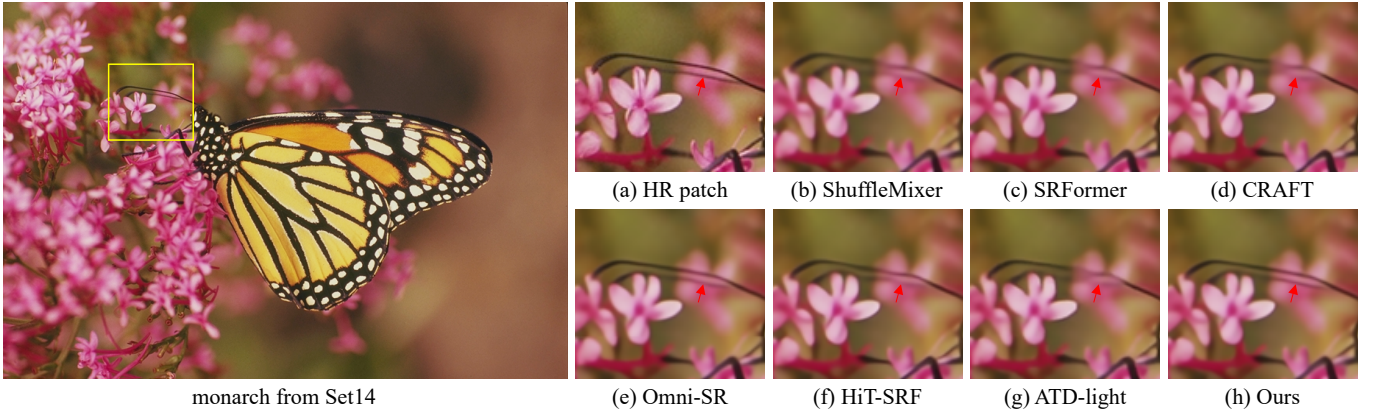


Fig. 5: Visual comparison of  $\times 4$  SR on Set14. The proposed SSIU shows clearer structural details.

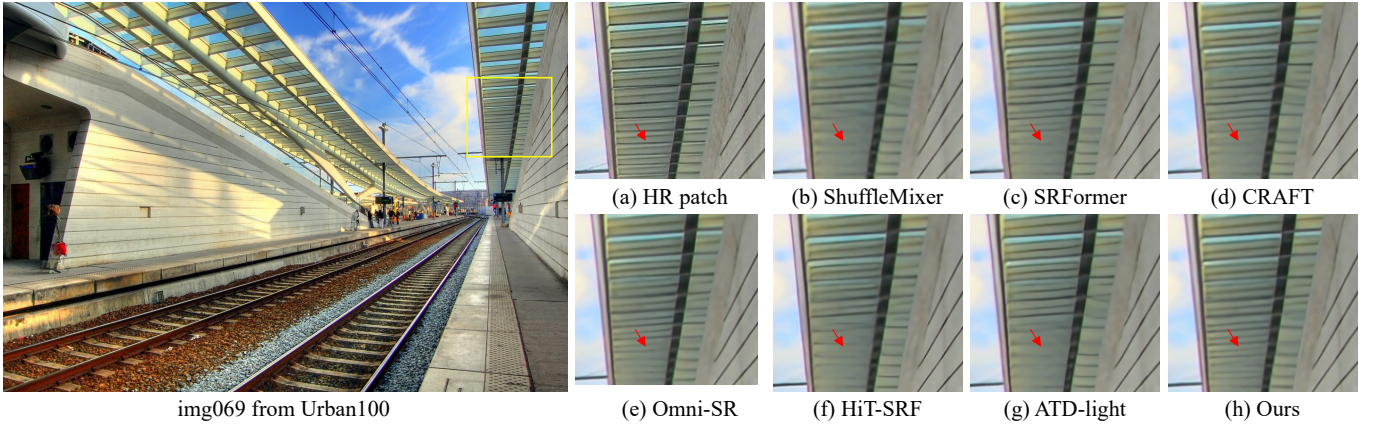


Fig. 6: Visual comparison of  $\times 4$  SR on Urban100. The proposed SSIU shows clearer structural details.

TABLE III: Performance comparison with and without the MOE-FS and ESAM. SAM denotes the self-attention module.

ESAM	SAM	MOE-FS	Flops	Param.	Set5		Set14		B100		Urban100		Manga109	
					PSNR	SSIM	PSNR	SSIM	PSNR	SSIM	PSNR	SSIM	PSNR	SSIM
✓			48	777.83	32.42	0.9012	28.88	0.7818	27.76	0.7452	26.63	0.8029	31.29	0.9210
✓		✓	49	794.47	32.64	0.9032	28.96	0.7939	27.82	0.7472	26.83	0.8098	31.60	0.9242
	✓	✓	54	788.71	32.62	0.9031	28.99	0.7944	27.83	0.7473	26.90	0.8106	31.64	0.9247

average inference time is computed over 100 SR images of resolution  $480 \times 320$  pixels, evaluated on an NVIDIA GeForce RTX 4090 GPU. As shown in Table II, our method achieves the lowest average inference time and the least GPU memory consumption among all compared models. These results confirm that our approach introduces minimal computational overhead while delivering superior performance, underscoring the effectiveness of the proposed SSIU framework in reducing model complexity without compromising quality.

### C. Ablation Studies and Discussions

To better understand the workings of SSIU, we conduct comprehensive ablation studies to evaluate the roles of its various components, discussing their functionalities, contributions, and key parameter choices.

1) *Effectiveness of the MoE-FS*: To validate the effectiveness of the proposed MoE-FS module, we perform ablation

studies, as presented in the first and second rows of Table III. Although integrating MoE-FS introduces a slight increase in model parameters and computational complexity, it yields significant performance improvements across all benchmark datasets. These results demonstrate that aggregating multi-level features through the MoE-FS mechanism is beneficial for enhancing SR performance.

2) *Effectiveness of the ESAM*: In this experiment, we investigate the impact of the sparsity operation in the proposed ESAM on performance, comparing it with the traditional self-attention module (SAM) that does not incorporate sparsity. From the results presented in the second and third rows of Table III, we draw the following conclusions: Firstly, the sparsity operation in ESAM significantly reduces the computed feature quantity by eliminating redundant information while retaining the most informative features, reducing Flops by 10.2% compared to SAM. Secondly, compared with the



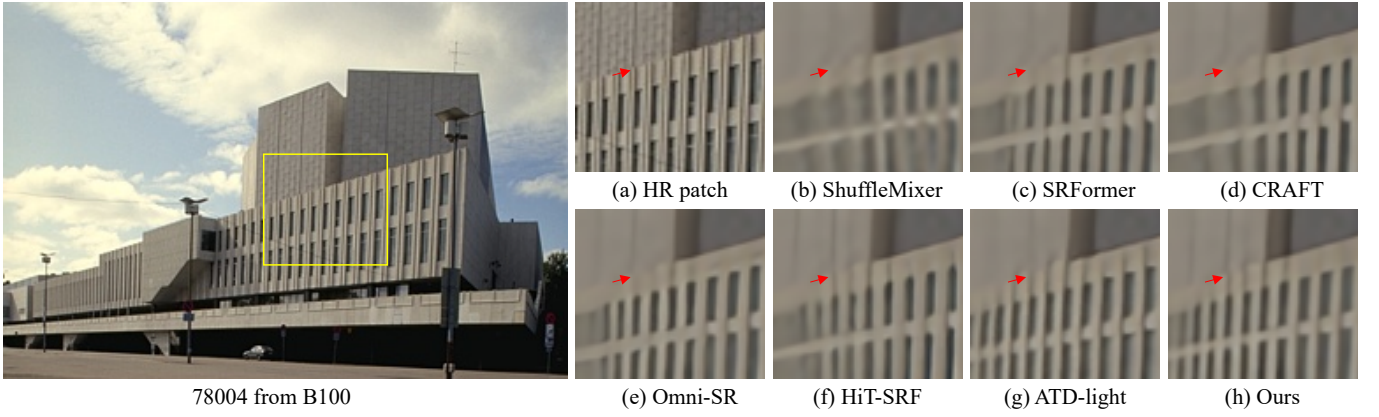


Fig. 7: Visual comparison of  $\times 4$  SR on B100. The proposed SSIU shows clearer structural details.

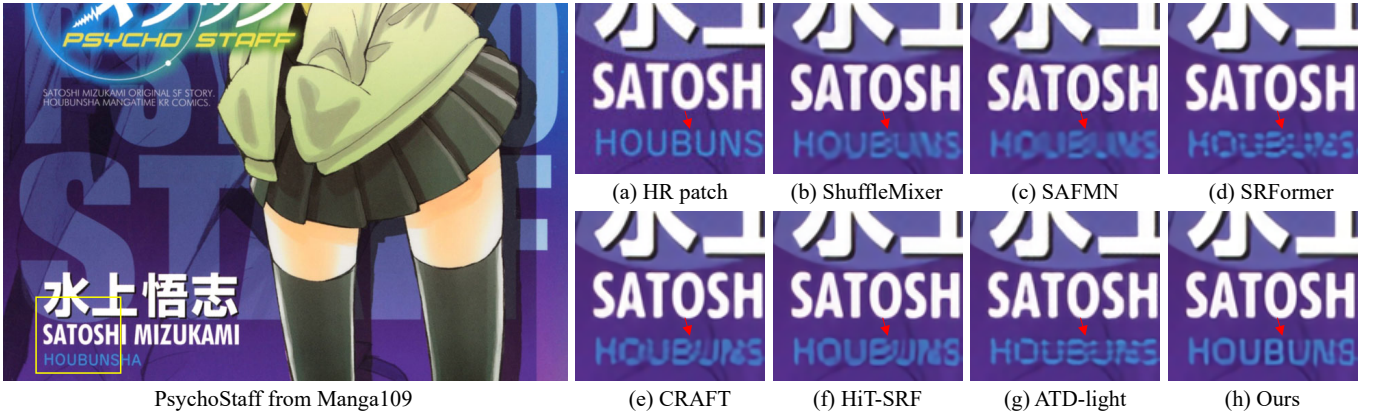


Fig. 8: Visual comparison of  $\times 4$  SR on Manga109. The proposed SSIU shows clearer structural details.

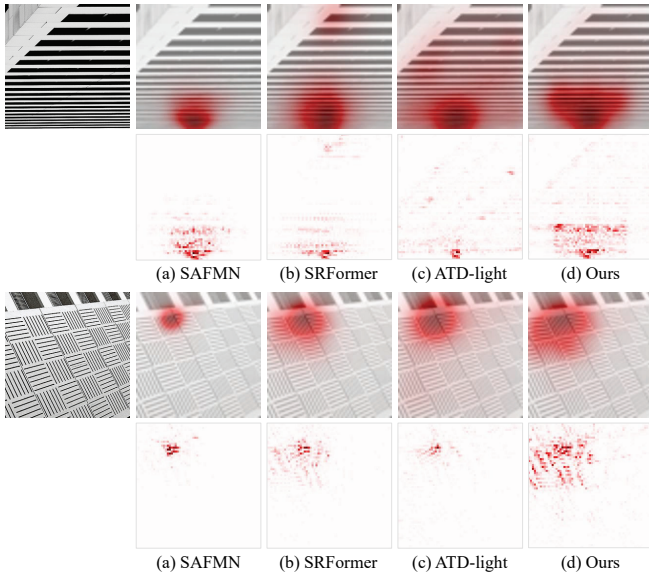


Fig. 9: Visual comparison of local attribution maps (LAM) of multiple methods in the same target area.

traditional self-attention module, the proposed ESAM maintains the performance on multiple benchmarks with a slight decrease. This shows that only long-distance information with

a similar structure is needed to reconstruct the current pixel information, which effectively proves the rationality of our method. To analyze the information aggregation capability of ESAM, we utilize local attribution maps (LAM) [59], a visualization tool that identifies pixels strongly influencing SR results, also known as information regions. Larger information regions indicate better aggregation ability. As shown in Fig. 9, we compare the information regions of various methods within the same target area. Our method demonstrates a larger information region than the others, highlighting that ESAM is more effective at modeling long-distance context using the attention mechanism.

3) *Effectiveness of the FFT Loss*: Previous studies usually optimize neural networks using the  $L_1$  distance. However, in this work, we explore the use of L1 distance in the frequency domain to encourage the network to focus more on high frequencies. From the results presented in Table IV, it can be observed that the FFT loss contributes to the improved performance of our network.

## V. CONCLUSION

Deep learning methods in SR often focus on enlarging the receptive fields to enhance performance, which can lead to increased model complexity. Our work seeks to develop a more effective method by activating pixels more sparsely. We employ an optimization function inspired by nonlocal

TABLE IV: Performance comparison of variants of different loss functions.

loss	Flops	Param.	Set5		Set14		B100		Urban100		Manga109	
			PSNR	SSIM	PSNR	SSIM	PSNR	SSIM	PSNR	SSIM	PSNR	SSIM
$L_1$	49	794.47	32.56	0.9022	28.87	0.7928	27.79	0.7468	26.81	0.8096	31.44	0.9234
$L_1 + \lambda L_f$	49	794.47	32.64	0.9032	28.96	0.7939	27.82	0.7472	26.83	0.8098	31.60	0.9242

structural similarity to build a lightweight SR network. By adopting an unfolding paradigm, our model establishes a step-by-step iterative process. In this process, mixed-scale gating modules and a sparse attention module are applied together; the former imposes sparsity and structural similarity constraints, while the latter achieves sparse long-range modeling. Additionally, we introduce a mixture-of-experts-based feature selector to gate feature information across different scales. Extensive experiments demonstrate that our unfolding-inspired network achieves both effectiveness and efficiency, outperforming current state-of-the-art models in terms of performance and inference time.

## REFERENCES

- [1] C. Dong, C. C. Loy, K. He, and X. Tang, "Image Super-Resolution Using Deep Convolutional Networks," *IEEE Transactions on Pattern Analysis and Machine Intelligence*, vol. 38, no. 2, pp. 295–307, 2015.
- [2] J. Kim, J. K. Lee, and K. M. Lee, "Accurate Image Super-Resolution Using Very Deep Convolutional Networks," in *Proceedings of the IEEE Conference on Computer Vision and Pattern Recognition*, 2016, pp. 1646–1654.
- [3] Q. Cai, J. Li, H. Li, Y.-H. Yang, F. Wu, and D. Zhang, "TDPN: Texture and Detail-Preserving Network for Single Image Super-Resolution," *IEEE Transactions on Image Processing*, vol. 31, pp. 2375–2389, 2022.
- [4] Y. Zhang, K. Li, K. Li, L. Wang, B. Zhong, and Y. Fu, "Image Super-Resolution Using Very Deep Residual Channel Attention Networks," in *Proceedings of the European Conference on Computer Vision*, 2018, pp. 286–301.
- [5] T. Dai, J. Cai, Y. Zhang, S.-T. Xia, and L. Zhang, "Second-Order Attention Network for Single Image Super-Resolution," in *Proceedings of the IEEE/CVF Conference on Computer Vision and Pattern Recognition*, 2019, pp. 11065–11074.
- [6] B. Niu, W. Wen, W. Ren, X. Zhang, L. Yang, S. Wang, K. Zhang, X. Cao, and H. Shen, "Single Image Super-Resolution via a Holistic Attention Network," in *Proceedings of the European Conference on Computer Vision*. Springer, 2020, pp. 191–207.
- [7] Y. Huang, J. Li, X. Gao, Y. Hu, and W. Lu, "Interpretable Detail-Fidelity Attention Network for Single Image Super-Resolution," *IEEE Transactions on Image Processing*, vol. 30, pp. 2325–2339, 2021.
- [8] P. Xu, Q. Liu, H. Bao, R. Zhang, L. Gu, and G. Wang, "FDSR: An Interpretable Frequency Division Stepwise Process Based Single-Image Super-Resolution Network," *IEEE Transactions on Image Processing*, 2024.
- [9] Z. Ni, R. Xiao, W. Yang, H. Wang, Z. Wang, L. Xiang, and L. Sun, "M2Trans: Multi-Modal Regularized Coarse-to-Fine Transformer for Ultrasound Image Super-Resolution," *IEEE Journal of Biomedical and Health Informatics*, 2024.
- [10] Z. Lu, J. Li, H. Liu, C. Huang, L. Zhang, and T. Zeng, "Transformer for Single Image Super-Resolution," in *Proceedings of the IEEE/CVF Conference on Computer Vision and Pattern Recognition*, 2022, pp. 457–466.
- [11] J. Liang, J. Cao, G. Sun, K. Zhang, L. Van Gool, and R. Timofte, "SwinIR: Image Restoration Using Swin Transformer," in *Proceedings of the IEEE/CVF International Conference on Computer Vision*, 2021, pp. 1833–1844.
- [12] Q. Cai, Y. Qian, J. Li, J. Lyu, Y.-H. Yang, F. Wu, and D. Zhang, "HIPA: Hierarchical Patch Transformer for Single Image Super Resolution," *IEEE Transactions on Image Processing*, vol. 32, pp. 3226–3237, 2023.
- [13] W. Shi, J. Caballero, F. Huszár, J. Totz, A. P. Aitken, R. Bishop, D. Rueckert, and Z. Wang, "Real-Time Single Image and Video Super-Resolution Using an Efficient Sub-Pixel Convolutional Neural Network," in *Proceedings of the IEEE Conference on Computer Vision and Pattern Recognition*, 2016, pp. 1874–1883.
- [14] L. Zhang, P. Wang, C. Shen, L. Liu, W. Wei, Y. Zhang, and A. Van Den Hengel, "Adaptive Importance Learning for Improving Lightweight Image Super-Resolution Network," *International Journal of Computer Vision*, vol. 128, no. 2, pp. 479–499, 2020.
- [15] N. Xu, X. Chen, Y. Cao, and W. Zhang, "Hybrid Post-Training Quantization for Super-Resolution Neural Network Compression," *IEEE Signal Processing Letters*, vol. 30, pp. 379–383, 2023.
- [16] Y. Zhang, H. Chen, X. Chen, Y. Deng, C. Xu, and Y. Wang, "Data-free Knowledge Distillation for Image Super-Resolution," in *Proceedings of the IEEE/CVF Conference on Computer Vision and Pattern Recognition*, 2021, pp. 7852–7861.
- [17] K. Zhang, Y. Li, W. Zuo, L. Zhang, L. Van Gool, and R. Timofte, "Plug-and-Play Image Restoration with Deep Denoiser Prior," *IEEE Transactions on Pattern Analysis and Machine Intelligence*, vol. 44, no. 10, pp. 6360–6376, 2021.
- [18] K. Zhang, W. Zuo, and L. Zhang, "Deep Plug-and-Play Super-Resolution for Arbitrary Blur Kernels," in *Proceedings of the IEEE/CVF Conference on Computer Vision and Pattern Recognition*, 2019, pp. 1671–1681.
- [19] M. Zhou, K. Yan, J. Pan, W. Ren, Q. Xie, and X. Cao, "Memory-Augmented Deep Unfolding Network for Guided Image Super-Resolution," *International Journal of Computer Vision*, vol. 131, no. 1, pp. 215–242, 2023.
- [20] X. Chen, X. Wang, J. Zhou, Y. Qiao, and C. Dong, "Activating More Pixels in Image Super-Resolution Transformer," in *Proceedings of the IEEE/CVF Conference on Computer Vision and Pattern Recognition*, 2023, pp. 22367–22377.
- [21] W. Dong, L. Zhang, G. Shi, and X. Wu, "Image Deblurring and Super-Resolution by Adaptive Sparse Domain Selection and Adaptive Regularization," *IEEE Transactions on Image Processing*, vol. 20, no. 7, pp. 1838–1857, 2011.
- [22] Y. Tai, J. Yang, and X. Liu, "Image Super-Resolution via Deep Recursive Residual Network," in *Proceedings of the IEEE Conference on Computer Vision and Pattern Recognition*, 2017, pp. 3147–3155.
- [23] Q. Yan, A. Niu, C. Wang, W. Dong, M. Woźniak, and Y. Zhang, "KGSr: A kernel guided network for real-world blind super-resolution," *Pattern Recognition*, vol. 147, p. 110095, 2024.
- [24] A. Dosovitskiy, L. Beyer, A. Kolesnikov, D. Weissenborn, X. Zhai, T. Unterthiner, M. Dehghani, M. Minderer, G. Heigold, S. Gelly *et al.*, "An Image is Worth 16x16 Words: Transformers for Image Recognition at Scale," in *Proceedings of the International Conference on Learning Representations*, 2020, pp. 1–21.
- [25] F. Yang, H. Yang, J. Fu, H. Lu, and B. Guo, "Learning Texture Transformer Network for Image Super-Resolution," in *Proceedings of the IEEE/CVF Conference on Computer Vision and Pattern Recognition*, 2020, pp. 5791–5800.
- [26] J. Yoo, T. Kim, S. Lee, S. H. Kim, H. Lee, and T. H. Kim, "Enriched Cnn-Transformer Feature Aggregation Networks for Super-Resolution," in *Proceedings of the IEEE/CVF Winter Conference on Applications of Computer Vision*, 2023, pp. 4956–4965.
- [27] L. Zhang, Y. Li, X. Zhou, X. Zhao, and S. Gu, "Transcending the Limit of Local Window: Advanced Super-Resolution Transformer with Adaptive Token Dictionary," in *Proceedings of the IEEE/CVF Conference on Computer Vision and Pattern Recognition*, 2024, pp. 2856–2865.
- [28] Q. Yan, K. Yang, T. Hu, G. Chen, K. Dai, P. Wu, W. Ren, and Y. Zhang, "From Dynamic to Static: Stepwisely Generate HDR Image for Ghost Removal," *IEEE Transactions on Circuits and Systems for Video Technology*, vol. 35, no. 2, pp. 1409–1421, 2025.
- [29] Q. Yan, T. Hu, P. Wu, D. Dai, S. Gu, W. Dong, and Y. Zhang, "Efficient Image Enhancement with A Diffusion-Based Frequency Prior," *IEEE Transactions on Circuits and Systems for Video Technology*, 2025.

- [30] A. Niu, T. X. Pham, K. Zhang, J. Sun, Y. Zhu, Q. Yan, I. S. Kweon, and Y. Zhang, "ACDMSR: Accelerated Conditional Diffusion Models for Single Image Super-Resolution," *IEEE Transactions on Broadcasting*, vol. 70, pp. 492–504, 2024.
- [31] Y. Wang, W. Yang, X. Chen, Y. Wang, L. Guo, L.-P. Chau, Z. Liu, Y. Qiao, A. C. Kot, and B. Wen, "SinSR: Diffusion-Based Image Super-Resolution in A Single Step," in *Proceedings of the IEEE/CVF Conference on Computer Vision and Pattern Recognition*, 2024, pp. 25 796–25 805.
- [32] B. Lim, S. Son, H. Kim, S. Nah, and K. Mu Lee, "Enhanced Deep Residual Networks for Single Image Super-Resolution," in *Proceedings of the IEEE Conference on Computer Vision and Pattern Recognition Workshops*, 2017, pp. 136–144.
- [33] N. Ahn, B. Kang, and K.-A. Sohn, "Fast, Accurate, and Lightweight Super-Resolution with Cascading Residual Network," in *Proceedings of the European Conference on Computer Vision*, 2018, pp. 252–268.
- [34] Z. Hui, X. Gao, Y. Yang, and X. Wang, "Lightweight Image Super-Resolution with Information Multi-Distillation Network," in *Proceedings of the 27th ACM International Conference on Multimedia*, 2019, pp. 2024–2032.
- [35] W. Li, K. Zhou, L. Qi, N. Jiang, J. Lu, and J. Jia, "LAPAR: Linearly-Assembled Pixel-Adaptive Regression Network for Single Image Super-Aesolution and Beyond," *Proceedings of the Advances in Neural Information Processing Systems*, vol. 33, pp. 20 343–20 355, 2020.
- [36] X. Zhang, H. Zeng, and L. Zhang, "Edge-oriented Convolution Block for Real-time Super Resolution on Mobile Devices," in *Proceedings of the 29th ACM International Conference on Multimedia*, 2021, pp. 4034–4043.
- [37] L. Wang, X. Dong, Y. Wang, X. Ying, Z. Lin, W. An, and Y. Guo, "Exploring Sparsity in Image Super-Resolution for Efficient Inference," in *Proceedings of the IEEE/CVF Conference on Computer Vision and Pattern Recognition*, 2021, pp. 4917–4926.
- [38] L. Sun, J. Pan, and J. Tang, "ShuffleMixer: An Efficient ConvNet for Image Super-Resolution," *Proceedings of the Advances in Neural Information Processing Systems*, vol. 35, pp. 17 314–17 326, 2022.
- [39] G. Gao, Z. Wang, J. Li, W. Li, Y. Yu, and T. Zeng, "Lightweight Bimodal Network for Single-Image Super-Resolution via Symmetric CNN and Recursive Transformer," in *Proceedings of the International Joint Conference on Artificial Intelligence*, 2022, pp. 913–919.
- [40] Y. Zhou, Z. Li, C.-L. Guo, S. Bai, M.-M. Cheng, and Q. Hou, "SR-Former: Permuted Self-Attention for Single Image Super-Resolution," in *Proceedings of the IEEE/CVF International Conference on Computer Vision*, 2023, pp. 12 780–12 791.
- [41] A. Li, L. Zhang, Y. Liu, and C. Zhu, "Feature Modulation Transformer: Cross-Refinement of Global Representation via High-Frequency Prior for Image Super-Resolution," in *Proceedings of the IEEE/CVF International Conference on Computer Vision*, 2023, pp. 12 514–12 524.
- [42] L. Sun, J. Dong, J. Tang, and J. Pan, "Spatially-Adaptive Feature Modulation for Efficient Image Super-Resolution," in *Proceedings of the IEEE/CVF International Conference on Computer Vision*, 2023, pp. 13 190–13 199.
- [43] H. Wang, X. Chen, B. Ni, Y. Liu, and J. Liu, "Omni Aggregation Networks for Lightweight Image Super-Resolution," in *Proceedings of the IEEE/CVF Conference on Computer Vision and Pattern Recognition*, 2023, pp. 22 378–22 387.
- [44] X. Zhang, Y. Zhang, and F. Yu, "HiT-SR: Hierarchical Transformer for Efficient Image Super-Resolution," in *Proceedings of the European Conference on Computer Vision*, 2024, pp. 483–500.
- [45] W. Dong, L. Zhang, G. Shi, and X. Li, "Nonlocally Centralized Sparse Representation for Image Restoration," *IEEE Transactions on Image Processing*, vol. 22, no. 4, pp. 1620–1630, 2012.
- [46] R. He, W.-S. Zheng, T. Tan, and Z. Sun, "Half-Quadratic-based Iterative Minimization for Robust Sparse Representation," *IEEE Transactions on Pattern Analysis and Machine Intelligence*, vol. 36, no. 2, pp. 261–275, 2013.
- [47] I. Daubechies, M. Defrise, and C. De Mol, "An Iterative Thresholding Algorithm for Linear Inverse Problems with a Sparsity Constraint," *Communications on Pure and Applied Mathematics: A Journal Issued by the Courant Institute of Mathematical Sciences*, vol. 57, no. 11, pp. 1413–1457, 2004.
- [48] X. Zhang, H. Dong, Z. Hu, W.-S. Lai, F. Wang, and M.-H. Yang, "Gated Fusion Network for Degraded Image Super Resolution," *International Journal of Computer Vision*, vol. 128, pp. 1699–1721, 2020.
- [49] J. Zhou, P. Wang, J. Tang, F. Wang, Q. Liu, H. Li, and R. Jin, "What Limits the Performance of Local Self-attention?" *International Journal of Computer Vision*, pp. 1–13, 2023.
- [50] J.-N. Su, M. Gan, G.-Y. Chen, W. Guo, and C. P. Chen, "High-Similarity-Pass Attention for Single Image Super-Resolution," *IEEE Transactions on Image Processing*, 2024.
- [51] E. Agustsson and R. Timofte, "NTIRE 2017 Challenge on Single Image Super-Resolution: Dataset and Study," in *Proceedings of the IEEE Conference on Computer Vision and Pattern Recognition Workshops*, 2017, pp. 126–135.
- [52] M. Bevilacqua, A. Roumy, C. Guillemot, and M. L. Alberi-Morel, "Low-Complexity Single-Image Super-Resolution Based on Nonnegative Neighbor Embedding," in *Proceedings of the British Machine Vision Conference*, 2012, pp. 1–10.
- [53] R. Zeyde, M. Elad, and M. Protter, "On Single Image Scale-Up Using Sparse-Representations," in *Proceedings of the International Conference on Curves and Surfaces*. Springer, 2010, pp. 711–730.
- [54] D. Martin, C. Fowlkes, D. Tal, and J. Malik, "A Database of Human Segmented Natural Images and Its Application to Evaluating Segmentation Algorithms and Measuring Ecological Statistics," in *Proceedings of the IEEE International Conference on Computer Vision*, vol. 2, 2001, pp. 416–423.
- [55] J.-B. Huang, A. Singh, and N. Ahuja, "Single Image Super-Resolution from Transformed Self-Exemplars," in *Proceedings of the IEEE Conference on Computer Vision and Pattern Recognition*, 2015, pp. 5197–5206.
- [56] Y. Matsui, K. Ito, Y. Aramaki, A. Fujimoto, T. Ogawa, T. Yamasaki, and K. Aizawa, "Sketch-Based Manga Retrieval using Manga109 Dataset," *Multimedia Tools and Applications*, vol. 76, pp. 21 811–21 838, 2017.
- [57] D. P. Kingma and J. Ba, "Adam: A method for stochastic optimization," in *Proceedings of the International Conference on Learning Representations*, 2015.
- [58] I. Loshchilov and F. Hutter, "SGDR: Stochastic Gradient Descent with Warm Restarts," in *Proceedings of the International Conference on Learning Representations*, 2017, pp. 1–16.
- [59] J. Gu and C. Dong, "Interpreting Super-Resolution Networks with Local Attribution Maps," in *Proceedings of the IEEE/CVF Conference on Computer Vision and Pattern Recognition*, 2021, pp. 9199–9208.